Operando Observation of the Gold−Electrolyte Interface in Li−O$_2$ Batteries

Forrest S. Gittleson, Won-Hee Ryu, and André D. Taylor*

Department of Chemical and Environmental Engineering, Yale University, 9 Hillhouse Avenue, New Haven, Connecticut, United States

Ⓢ Supporting Information

ABSTRACT: Observing the cathode interface in Li−O$_2$ batteries during cycling is necessary to improve our understanding of discharge product formation and evolution in practical cells. In this work a gold electrode surface is monitored by operando surface-enhanced Raman spectroscopy during typical discharge and charge cycling. During discharge, we observe the precipitation of stable and reversible lithium superoxide (LiO$_2$), in contrast to reports that suggest it is a mere intermediate in the formation of lithium peroxide (Li$_2$O$_2$). Some LiO$_2$ is further reduced to Li$_2$O$_2$ producing a coating of insulating discharge products that renders the gold electrode inactive. Upon charging, a superficial layer of these species (∼1 nm) are preferentially oxidized at low overpotentials (<0.6 V), leaving residual products in poor contact with the electrode surface. In situ electrochemical impedance spectroscopy is also used to distinguish between LiO$_2$ and Li$_2$O$_2$ products using frequency-dependent responses and to correlate their reduction and oxidation potentials to the accepted mechanism of Li$_2$O$_2$ formation. These operando and in situ studies of the oxygen electrode interface, coupled with ex situ characterization, illustrate that the composition of discharge products and their proximity to the catalytic surface are important factors in the reversibility of Li−O$_2$ cells.

KEYWORDS: lithium−oxygen, lithium−air, Li$_2$O$_2$, LiO$_2$, SERS, Raman spectroscopy, electrochemical impedance spectroscopy
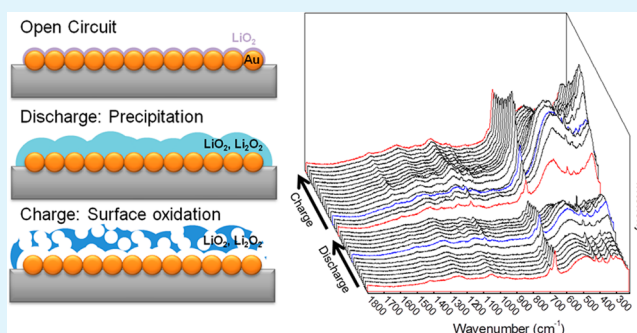
INTRODUCTION

The lithium−oxygen battery is an emerging energy storage system promising up to ten times the theoretical energy density of standard lithium-ion cells,[1−4] yet few studies have been able to demonstrate why this theoretical prediction has not been realized. Cell degradation mechanisms have been suggested for systems of differing electrolytes and electrode materials ranging from the formation of irreversible side products,[5−8] to poor kinetics,[9,10] to poor electrical conductivity of the discharge products.[11−14] Recently, several studies have observed the impact of cycling rate on the morphology, stoichiometry, and reversibility of the discharge products.[15−19] To obtain insight into the reduction and oxidation processes, especially at the oxygen electrode surface, it is necessary to perform in situ studies.

While several studies have examined the electrochemical phenomena in situ at the electrode interface using transmission electron microscopy (TEM),[20] atomic force microscopy (AFM),[21,22] X-ray photoelectron spectroscopy (XPS)[23,24] and Raman spectroscopy,[25,26] none can be considered operando,[27] that is utilizing a cell environment and settings that lack compromises for characterization. Compromises common for in situ studies include the use of nonstandard electrolytes (i.e., LiPON and ionic liquids), electrodes preloaded with discharge products, and apparatuses that require an open environment. To date, only differential electrochemical mass spectroscopy

(DEMS) has been applied with an operando methodology in Li−O$_2$ cells,[6,28−30] but data collection is limited to the monitoring of gaseous products and not the electrode surface.

Catalysts for oxygen reduction and evolution are beginning to be recognized as necessary to lower the reaction overpotentials in Li−O$_2$ cells.[31−33] Previous studies have shown that carbon electrodes degrade upon cycling forming poorly reversible side products,[7] but metals such as Au, Pt, Pd, and Ru may catalyze oxygen reduction and evolution with limited side reactions.[30,34−37] The use of carbon-free all-metal electrodes provides the opportunity to precisely study catalyst−electrolyte interfacial phenomena during cycling, as well as reduce overpotentials and improve the cycle life of Li−O$_2$ cells.[30]

Here we observe the precipitation and evolution of discharge products on an Au electrode surface by combined operando and in situ surface spectroscopy. Surface-enhanced Raman spectroscopy (SERS) provides a relatively facile probe of the electrode interface without significant perturbation to the system.[38−42] Previously, Peng et al. employed in situ Raman spectroscopy with a potentiostatic method focused on establishing a mechanism of product formation and evolution

over very short time scales, but this study did not look at practical cell phenomena over full cycles.[25] The work presented here shows that with standard galvanostatic cycling, a more practical electrolyte solvent (DMSO vs acetonitrile) and an operando methodology, Raman signals from the electrolyte, discharge products, and the electrode itself can be distinguished to provide insight into product flux, stoichiometry, and proximity to the catalyst surface. In contrast to previous reports which show LiO_2 is an intermediate in the formation of Li_2O_2, we observe the formation of stable and reversible LiO_2 consistent with reduced overpotentials of cycling. We also show that in situ electrochemical impedance spectroscopy (EIS) can elucidate Li–O_2 reaction mechanisms by distinguishing between discharge species and the electrochemical potentials of their formation and evolution. Paired with ex situ morphological characterization, these methods provide a more complete picture of the flux of discharge products on catalyst surfaces and explain that incomplete oxidation due to poor surface contact is a common failure mechanism in these Li–O_2 cells.

■ EXPERIMENTAL SECTION

Sample Preparation. Oxygen electrodes were prepared starting from a flattened 12.7 mm diameter Ni foam substrate. Following cleaning by sonication in ethanol and acetone to remove organic residue, Ni foams were reacted with a 2.5 mL solution of 2 mM $HAuCl_4$ (Sigma-Aldrich) in water by galvanic displacement for 2 h to achieve a 1 mg dense loading of ~75 nm Au particles. Electrodes were removed from the solution, rinsed with DI water thoroughly and dried at 100 °C.

Li–O_2 cells were assembled inside an argon purged glovebox using a specifically designed cell described elsewhere.[9] A piece of 11.1 mm diameter Li foil was used as the counter electrode with a 13 mm diameter Whatman glass fiber separator. The separator was impregnated with approximately 60 μL of 0.1 M $LiClO_4$ (Sigma-Aldrich) in anhydrous DMSO (Alfa Aesar) or TEGDME (Sigma-Aldrich) solvent. Sealed cells were removed from the glovebox, purged several times with dry O_2 and resealed prior to cycling. Karl Fisher titration on the as-purchased anhydrous DMSO verified a water content of <50 ppm.

Raman Spectroscopy. The Li–O_2 optical cell used for operando SERS had the same structure as cells used for other cycling experiments except for the addition of a 0.4 mm thick sapphire window (Edmund Optics) at the center of the anode current collector. Small holes were cut in the Li foil anode and separator to allow an optical path to the oxygen electrode surface. The in-cell optical path length was ~1 mm. A schematic of the optical cell is provided in Figure S1 of the Supporting Information. Operando Raman spectroscopy was conducted using a Jasco 3100 laser Raman spectrophotometer with a 785 nm excitation wavelength. Spectra were measured over 120 s and averaged over 3 accumulations to improve resolution. Similar settings were employed for ex situ spectroscopy of cycled electrodes.

Electrochemical Characterization. A Biologic VSP potentiostat with impedance spectroscopy function was used for EIS measurements and galvanostatic cycling of cells. Impedance measurements were conducted using a staircase sequence from 3.0 to 2.0 V for the discharge followed by a 2 h rest period at open circuit potential and a second staircase sequence from 3.0 to 3.8 V for the charge. Impedance spectra were taken every 50 mV with an amplitude of 50 mV following a 2 min hold period at each potential. Galvanostatic cycling experiments were conducted with a rate of 50 μA (~12 mA/cm^2_{real}) for the discharge and 20 μA for the charge cycle for each electrode with a range of 2.0–3.8 V.

Physical Characterization. Ex situ physical characterization of pristine and cycled electrodes was conducted using an FEI Tecnai Osiris 200 kV transmission electron microscope (TEM) and a Hitachi SU-70 scanning electron microscope (SEM) with energy dispersive X-ray spectroscopy (EDS) functions. XRD was also used to evaluate

crystallinity. X-ray photoelectron spectroscopy (XPS) measurements were performed at Brookhaven National Laboratory on a SPECS GmbH instrument under ultrahigh vacuum (UHV) conditions. The X-ray source was Al Kα at a power of 300 W. Data were collected for C 1s, O 1s, and Au 4f with a pass energy of 25 eV. The binding energies of Au–Ni foam pristine and Li^+/DMSO treated Au–Ni foam samples were calibrated to the C 1s photoemission peak of adventitious hydrocarbons at 285.0 eV. The binding energies of discharged and charged samples were calibrated to the C 1s photoemission peak of Li_2CO_3 at 290.0 eV[24,43] because of the difficulty of distinguishing an adventitious hydrocarbon peak. Peak locations and peak widths were obtained using a Shirley background subtraction and by fitting the data to mixed Gaussian–Lorentzian line shapes (CasaXPS).

■ RESULTS AND DISCUSSION

Operando Raman Spectroscopy. Au-coated Ni-foam electrodes used for operando SERS were shown to provide exceptional enhancement of the Raman signal at low wavenumbers up to ~1500 cm^{-1}. Electrodes were loaded into a specifically designed cell with a sapphire window providing an optical path to the Au surface. A DMSO-based electrolyte was used because of the kinetic advantage it offers over ether-based electrolytes.[9,30] Cells were discharged and charged in the range 2.0–3.8 V to limit degradation of the electrolyte and the unprotected Li anode.[30,44]

We show (Figure 1) time-resolved Raman spectra for a typical Au–Ni foam/DMSO cell during the (a) first discharge and charge (front to back), and (b) second discharge (back to front). The evolution of the various Raman peaks can be observed during discharge and charge cycles. Following each discharge or charge step, the open circuit potential Raman spectra are provided in red. Accompanying discharge and charge profiles are available in the Supporting Information (S2). Features corresponding to the gold electrode (~500 cm^{-1}) and DMSO (most significantly 670, 700, and 1055 cm^{-1}) are evident along with a broad feature corresponding to the Ni foam substrate (~1255 cm^{-1}). A full table of Raman peak designations from literature and accompanying baseline spectra for as-purchased products are available in the Supporting Information (Table S1, Figure S3).

Changes in the intensity of Raman features relating to the Au surface, solvent, and Li–O_2 discharge products aids in understanding the interfacial phenomena. A high intensity of the Au electrode features specifically denotes the availability of that surface, whereas a low intensity suggests its coating with products. During discharging, the Au feature at ~500 cm^{-1} increases in intensity (along with its resonant peak at ~1000 cm^{-1}) around 2.65 V (Figure 1a blue spectrum), indicating a reorganization of the surface structure. We believe that this surface reorganization involves the reaction of an initial passivating film on the Au surface. We discovered evidence that this passivation layer may consist of a small amount of spontaneously generated superoxide (additional discussion below) and residual chlorides from the galvanic deposition procedure (Au–Cl feature at 275 cm^{-1}).[40] Also around 2.65 V, a Raman feature at 1140 cm^{-1} is introduced, corresponding to the LiO_2 stoichiometry reported previously.[25,45,46] While we do not observe a peak at ~790 cm^{-1} which would suggest the presence of Li_2O_2, it is probable that the intensity of this feature is quite low, consistent with generally lower Raman intensities for ionic bonding. We observe no distinct features related to LiOH (331 cm^{-1}) or Li_2CO_3 (1093 cm^{-1}) byproducts that have been reported as a consequence of impurities (i.e., water) or electrolyte decomposition. Several studies have observed Li_2SO_4
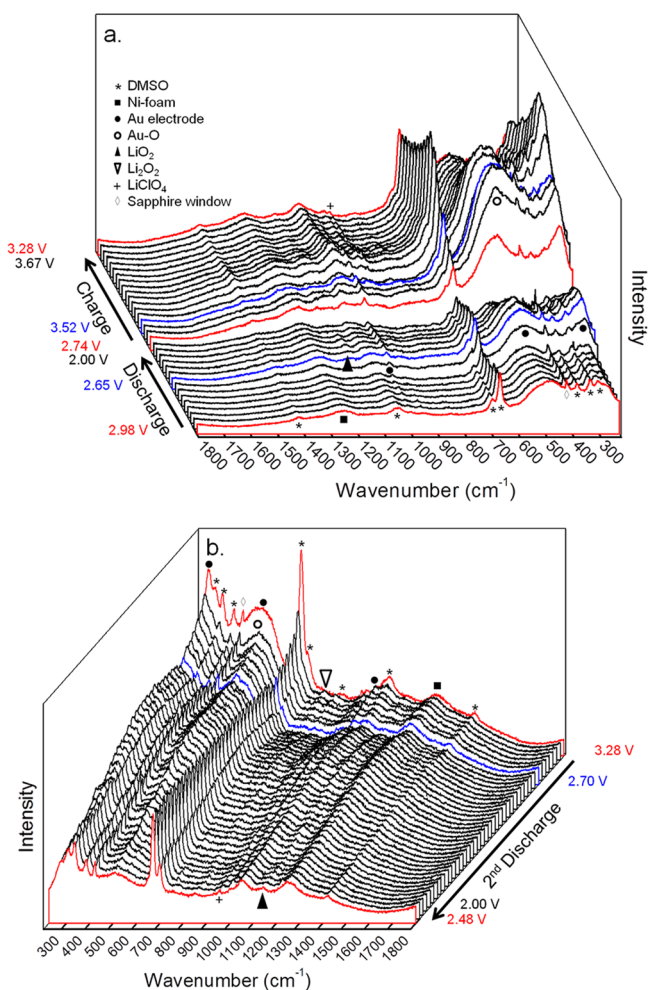
Figure 1. Operando Raman spectra of an Au−Ni foam electrode with a DMSO-based electrolyte. (a) first discharge and charge cycle (front to back) and (b) second discharge cycle (back to front). Red curves represent spectra taken at open circuit potential. Accompanying cycle profiles are available in the Supporting Information (S2).

or dimethyl sulfone ($DMSO_2$) byproducts from DMSO decomposition during cycling,[47−50] but we see no indication of these species (i.e., 1014 cm^{-1} for Li_2SO_4 or 501 and 706 cm^{-1} for $DMSO_2$) either during operando experiments or ex situ (see Table S1 in the Supporting Information). As the total experimental time is short (∼7 h) compared to other reports,[50] the formation of these side products is likely to be minimal. Also, the use of gold rather than high surface area carbon for the electrode has been shown to limit the decomposition of DMSO.[47] The fact that the Au electrode intensity is diminished toward the end of the discharge and accompanied by the growth of the LiO_2 feature indicates that the electrode surface is progressively covered with discharge products. A recent report illustrating the formation of Li_2O_2 by "late stage" disproportionation of LiO_2 provides a compelling rationale for the compaction of discharge products which leads to electrode deactivation.[51]

The application of anodic current to the Au electrode begins the charge cycle where we observe increases in intensity of the Au (∼500 cm^{-1}) and DMSO electrolyte features (most notably at 670 cm^{-1}). This indicates that the discharge products are rapidly removed from the Au surface. The highest intensity from the Au surface is achieved by 3.52 V (Figure 1a blue

spectrum in the charge region). By calculating the number of electrons recovered from the electrode by this point, we estimate that ∼0.6 nm of Li_2O_2 or ∼1.0 nm of LiO_2 has been removed from the surface. (A description of this calculation and its assumptions is included in the Supporting Information.) Although this limited evolution accounts for only 6% of the products formed upon discharge, it appears to effectively free the Au active surface from product coatings. We note that an in situ TEM study previously showed similar phenomena in which evolution of the discharge products occurs preferentially at a CNT surface.[20] Over the course of the charge cycle, the LiO_2 feature at 1140 cm^{-1} decreases in intensity indicating its removal from the Au surface. We suspect that evolution of bulk (non-superficial) discharge products occurs at higher potentials and constitutes the remainder of the charge cycle. This likely involves the migration or collapse of these products onto the electrode surface to facilitate oxygen evolution. While much previous work has focused on proving the generation and evolution of Li_2O_2, our operando data suggest that LiO_2 is not merely an intermediate, but a product that can be reversibly formed and evolved upon cycling. We speculate that any non-oxidized discharge products are largely disconnected from the electrode surface—a hypothesis supported by ex situ Raman and TEM characterization (see below).

A second discharge was conducted to observe the Au surface upon continued cycling (Figure 1b). A decrease in the intensity of Au features is once again observed along with a decrease in the DMSO signal, both indicating Au surface coating. We find that the DMSO intensities are relatively stable following an initial peak drop, which may indicate electrolyte trapped within the interfacial discharge product. Most surprisingly, we observe a feature at 791 cm^{-1} corresponding to Li_2O_2 in the initial stages of discharge. This feature later disappears as the LiO_2 feature at ∼1140 cm^{-1} increases and persists through the remainder of the discharge cycle. This result indicates that Li_2O_2 is formed in the first discharge cycle, and that residual Li_2O_2 not evolved during charging is in close proximity to the electrode surface at the start of the second discharge. As the new product layer forms at the Au interface, residual Li_2O_2 is pushed further away and its signal is lost. We conclude that discharge products disconnected from the surface during charging persist upon repeated cycles.

We also observe a shift in the peak position of the LiO_2 feature over the course of the discharge reaction. By plotting the peak wavenumber against the potential, a peak shift from ∼1138 to ∼1148 cm^{-1} is evident (S4), indicating a stiffening or shortening of the O−O superoxide bond. Compressive strain caused by the applied electric field and the precipitation of new products may account for this shift, but additional studies are necessary.

Raman spectroscopy using a TEGDME-based electrolyte shows similar Au surface coating and evolution (S5). We find that ∼6% of the discharge products are evolved by 3.36 V upon charging, corresponding to the highest intensity of the 500 cm^{-1} Au feature, similar to the result with a DMSO electrolyte. We conclude that surface product evolution is an effect of intimate contact between the discharge product and the Au surface, not merely an effect of the electrolyte selection.

Product Morphology. The morphology and stoichiometry of the discharge and charge species and their proximity to the electrode surface is important to discern because of its effect on reversibility. Full characterization of the as-synthesized Au electrode by Raman spectroscopy, XPS, and TEM imaging is presented in Figures 2, 3a, and 4a indicating only a pristine Au
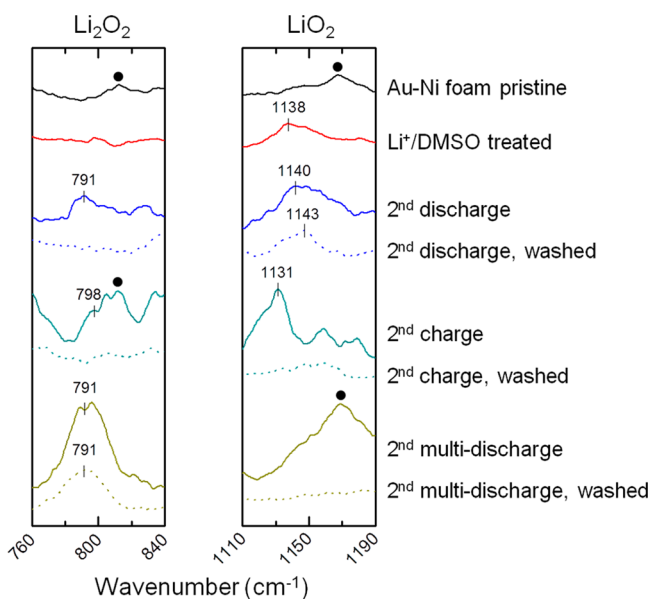
Figure 2. Ex situ Raman spectra of Au−Ni foam electrodes at different states of charge. Marked peaks denote the presence of Li_2O_2, LiO_2, or Au−Ni foam electrode features (●). Dotted lines represent spectra after washing electrodes with anhydrous DMSO.

surface (with typical adventitious hydrocarbons present in the XPS spectrum). Figure 2 also presents ex situ Raman spectra of Au electrodes following the second discharge and charge cycles. The second discharge and charge cycles were chosen to stress the importance of reversibility on Li−O$_2$ catalyst function and to eliminate any effects from the previously described initial passivation layer. Both Li_2O_2 and LiO_2 are detected on the discharged electrode, confirming that Li_2O_2 is present, albeit difficult to detect in our operando studies. Li_2O_2 was also detected by XPS (Figure 3c) in the O 1s spectrum (∼531.4 eV[23,24]) despite some contamination by CO_2 during sample transfer to UHV. The presence of a small feature in the discharged electrode O 1s spectrum corresponding to under-coordinated oxygen (i.e., O_2^{-2}, O^-) at ∼530.2 eV[23,52] is of particular interest, supporting the longer-term stability of "intermediate" species. There is some indication in the literature that two overlapping features centered at 531.5 eV (deconvoluted as 530.9 and 532.1 eV) would indicate the presence of superoxide,[53,54] but this would be difficult to distinguish from the rather broad feature we attribute to Li_2O_2. The presence of small amounts of LiOH (∼531.0 eV), as a product of DMSO decomposition, or Li_2O (528.6 eV) cannot be entirely eliminated by XPS[55] but neither were detected by ex situ Raman spectroscopy. Together, Raman and XPS provide complementary information that the composition of discharge species is likely a mixture of Li_2O_2 and LiO_2.

Ex situ Raman spectroscopy on the charged electrode similarly indicates the presence of Li_2O_2 and LiO_2 products (Figure 2). A LiO_2 feature with a wavenumber of 1131 cm^{-1} (vs 1140 cm^{-1} for the discharge) suggests a softening or lengthening of the O−O superoxide bond due to charging, which may support a less dense or relaxed product morphology. XPS data for the charged sample (Figure 3d) shows the presence of Li_2O_2 (∼531.3 eV) but no under-coordinated oxygen, indicating that these species were either evolved at low overpotentials or remain below the penetration depth of XPS (i.e., closer to the Au surface).

Both discharged and charged electrodes were washed in anhydrous DMSO to remove non-surface species and analyzed

once again by Raman spectroscopy (Figure 2 dotted lines). After washing, the Li_2O_2 Raman feature from the discharged sample is eliminated, suggesting that this species is weakly connected to the electrode surface. LiO_2 and Li_2O_2 are also removed from the charged electrode by washing, supporting the theory that charge products are disconnected from the electrode by preferential surface oxidation. Data from Li$^+$/DMSO treated and "multi-discharged" electrodes, a particular case of over-discharge, are discussed alongside EIS results below.

Ex situ TEM images of the Au electrode at different states of charge show that discharge products precipitate directly at the electrode interface (Figure 4). The formation of an amorphous layer of surface products during the second discharge (2.7 nm average thickness) is evident in Figure 4b. Following the second charge (Figure 4c), the average thickness of the interfacial layer is 1.6 nm, a reduction of ∼1.1 nm. This lends credence to our calculation that ∼1.0 nm of products is oxidized in the initial part of the charge cycle. We note that the uniform coating of charge products in Figure 4c is indicative of its morphology only after exposure to the 200 kV TEM beam. In fact, we observe that the original charge product morphology is much thicker (up to 80 nm from the surface) and porous but is rapidly compressed down to just a few nanometers of dense product due to evaporation of residual trapped electrolyte. Time-lapse TEM images illustrating this phenomenon are available in the Supporting Information (S6). The original morphology of the charge product was also captured rapidly before its collapse by SEM (S7c). X-ray diffraction patterns of discharged and charged electrodes exhibited no crystalline Li_2O_2 peaks, indicating that the discharge and charge species are largely amorphous in nature (S8), consistent with TEM imaging.

In Situ Impedance Spectroscopy. To better understand the mechanism of discharge and charge at the Au interface, we employed in situ electrochemical impedance spectroscopy to observe changes in electrode resistance. Impedance was measured over a range of frequencies from 10^5−0.05 Hz in progression from 3.0 to 2.0 V for the discharge and 3.0 to 3.8 V for the charge with 50 mV steps. The potential-dependent real impedance was plotted for a range of frequencies (Figure 5). Raw data is provided rather than a circuit model fit because we believe it is less prone to interpretive error. A Bode plot shows that phase shifts over the course of a discharge occur in three main frequency ranges and are related to distinct processes in the Li−O$_2$ cell (Figure 5a). The high-frequency range (10^3−10^4 Hz) is thought to refer to fast ion transfer corresponding to the Li anode interface while the mid- and low-frequency ranges (10−100 Hz and <1 Hz, respectively) correspond to phenomena at the oxygen electrode interface.[56] The mid-frequency range is believed to correspond to the formation of "intermediate" products and the low-frequency range to more stable products. The relation of frequency-based responses in EIS to the transport of various oxygen intermediates has been shown in a similar fashion for solid oxide fuel cells.[57,58] Relating the frequency responses to the generally accepted mechanism for discharge found in Scheme 1, we suggest that the mid-frequency range relates to the formation and evolution of LiO_2 and the low-frequency range relates to the same for Li_2O_2. For clarity, the mid- and low-frequency ranges are plotted separately with log scales and regions of interest are highlighted (Figure 5b−e). A selected high-frequency plot relating to the Li anode interfacial resistance is provided in the Supporting Information (S9) and demonstrates a general increase in resistance upon repeated cycling.
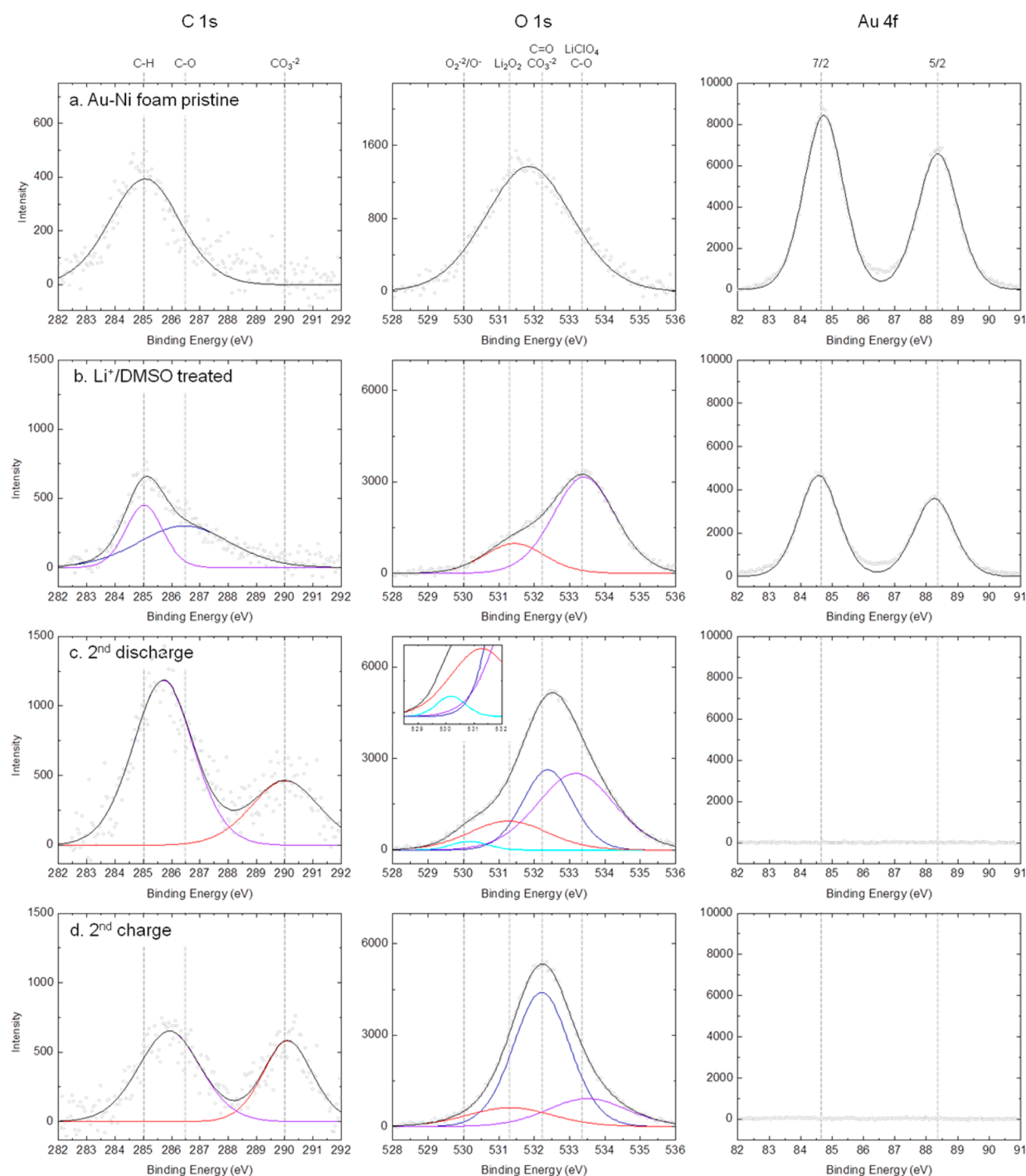
Figure 3. Ex situ X-ray photoelectron spectra of Au−Ni foam electrodes at different states of charge: (a) pristine, (b) electrolyte treated, (c) after discharge, and (d) after charge. Sample data fitted with Gaussian−Lorentzian line shapes (black line represents envelope fit). CO_3^{-2} and C=O attributions are likely the result of exposure to CO_2 during sample transfer.

The potential-dependent resistance data show distinguishing features related to the precipitation of "intermediate" and stable discharge product species (Figure 5b, c). For discharge, we highlight an increase in resistance in the mid-frequency range from 2.95 to 2.5 V followed by an increase in resistance in the low-frequency range from 2.7 to 2.4 V. This phenomena parallels the accepted mechanism for discharge whereby LiO_2 is first formed by reactions (1) and (2), then further reduced to Li_2O_2 by reactions (3a) or (3b). For consistency, the second cycle resistances (S10) were compared to those for the first cycle and show similar behavior. To test the validity of our

assumptions, a cell was also subjected to the same experimental conditions under Ar atmosphere (without O_2 purging). EIS data for this cell (S11) show no significant response during discharge, proving that the variation in resistance is directly related to the migration and/or reaction of oxygen species.

Our combined Raman and EIS results suggest that the initial discharge reactions (1) and (2) in Scheme 1 should be understood as surface reactions in which oxygen adsorbs first on the Au surface and then reacts with free Li^+ ions to form superficial LiO_2.[59,60] This is supported by the appearance of an Au−O feature related to surface adsorbed superoxide (481 cm^{-1}) in
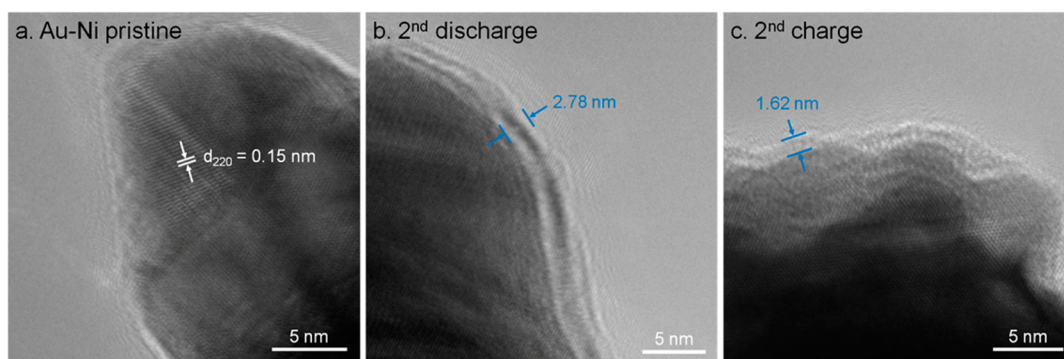
Figure 4. TEM images of the Au electrode surface: (a) pristine, (b) after discharge, and (c) after charge. Lattice spacing for Au is provided in a.
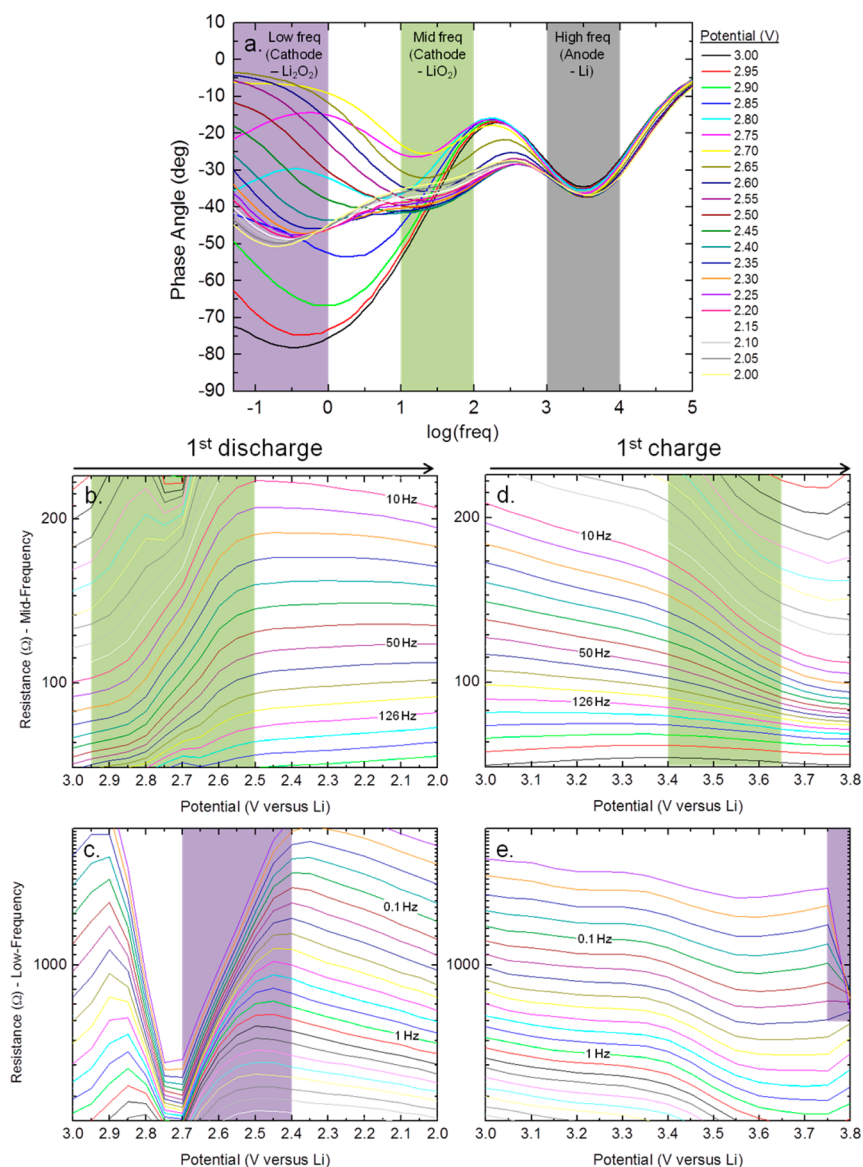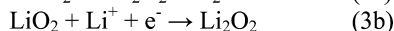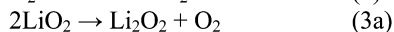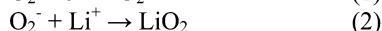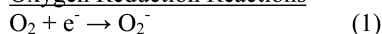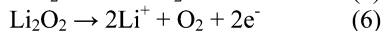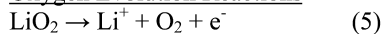

Figure 5. (a) Representative phase angle vs log(freq) indicating the regions which are correlated to different elements of the Li−O₂ cell. Potential dependent real resistance for (b, c) first discharge and (d, e) first charge cycle of an Au−Ni foam/DMSO cell where each line charts the resistance at a specific frequency. (b, d) mid-frequency range corresponding to resistance from LiO_2, (c, e) low-frequency range corresponding to resistance from Li_2O_2.

the second discharge Raman spectra at 2.73 V (Figure 1b). (The Au−O Raman peak is also apparent during the first charge cycle as O₂ is evolved from the surface products.)

The generation of adsorbed superoxide is likely the rate limiting reaction in accordance with the generally accepted mechanism. To evaluate the formation of the adsorbed superoxide species,

Scheme 1. [15,25,45]

Oxygen Reduction Reactions

$$O_2 + e^- \rightarrow O_2^- \tag{1}$$
$$O_2^- + Li^+ \rightarrow LiO_2 \tag{2}$$
$$2LiO_2 \rightarrow Li_2O_2 + O_2 \tag{3a}$$
$$LiO_2 + Li^+ + e^- \rightarrow Li_2O_2 \tag{3b}$$

Oxygen Evolution Reactions

$$LiO_2 \rightarrow Li^+ + O_2 + e^- \tag{5}$$
$$Li_2O_2 \rightarrow 2Li^+ + O_2 + 2e^- \tag{6}$$

we immersed a pristine Au−Ni foam electrode in a standard DMSO electrolyte with 0.1 M $LiClO_4$ for 10 min and dried it in low vacuum. The Raman spectra for this Li^+/DMSO treated electrode (Figure 2) shows a small feature at 1138 cm^{-1} indicating the presence of superficial LiO_2. XPS spectra for this sample (Figure 3b) under UHV conditions show the presence of Li_2O_2 (~531.4 eV), the expected product of LiO_2 disproportionation, or LiO_2, previously discussed as a possible deconvolution of the same feature. These data support the spontaneous reaction of residual adsorbed oxygen on Au with Li^+ ions in solution to form a thin passivation layer. Speculative reasoning for this phenomenon may be provided by studies on the interaction of O_2 with neutral Au clusters that demonstrate the spontaneous formation of superoxo-like states,[61,62] but additional in-depth studies are necessary.

EIS results for the first charge cycle (Figure 5d, e) show a subtle low-frequency decrease in resistance from 3.1 to 3.2 V, as well as a more gradual mid-frequency decrease in resistance from 3.0 to 3.4 V. We believe these are attributable to oxygen evolution from the surface of Li_2O_2 species[12,16,45] and from a layer of LiO_2 on the Au surface, respectively. A mid-frequency response in the range 3.4−3.65 V suggests bulk LiO_2 evolution (reaction (5) in Scheme 1) occurs preferentially at these potentials. Our finding that ~1.0 nm of products is removed from the Au surface at low overpotentials is consistent with this result. Bulk evolution of Li_2O_2 by reaction (6) is indicated by a decrease in resistance above 3.75 V in the low-frequency regime. This is accompanied by an increase in mid-frequency resistance suggesting that some Li_2O_2 may first decompose to LiO_2. Our selection of a 3.8 V cutoff potential explains why some Li_2O_2 remains near the electrode surface following charging.

To support our EIS data, we subjected cells with Au electrodes to standard high rate cycling and "multi-discharge" cycling. The multi-discharge cycling (similar to over-discharge, but within reasonable operating potentials) consisted of 10 discharge and rest periods that were then followed by a charge cycle and another 10 discharge and rest periods (S12a). The derivative capacity (dq/dt) of the charge, much like a cyclic voltammogram, can be correlated with the character of the discharge products formed in each case (S12b). Following a standard discharge, charge features are seen at 3.15, 3.55, and >3.8 V. After multi-discharge, the charge features are seen only at 3.55 and 3.75 V. The disappearance of the 3.15 V feature and subsequent increase in intensity of the 3.75 V feature with over-discharge indicates the growth and compaction of bulk Li_2O_2 on the Au surface. The fact that each subsequent discharge has a lower potential in the multi-discharge case, supports the notion that additional bulk Li_2O_2 is formed at low potentials[16] and evolved at high potentials (>3.75 V). This is confirmed by a comparison of the ex situ Raman spectra of standard and multi-discharged electrodes (Figure 2) in which the Li_2O_2 peak is more prevalent

for the multi-discharged electrode. SEM images of the multi-discharged electrode surface also show crystalline Li_2O_2 particles and a thicker product layer coating the Au surface (S7d).

Interfacial Discharge/Charge Scheme. Coupling operando Raman spectroscopy data with in situ EIS and ex situ characterization we propose the discharge/charge scheme seen in Figure 6. Upon discharging of the cell, LiO_2 species precipitate
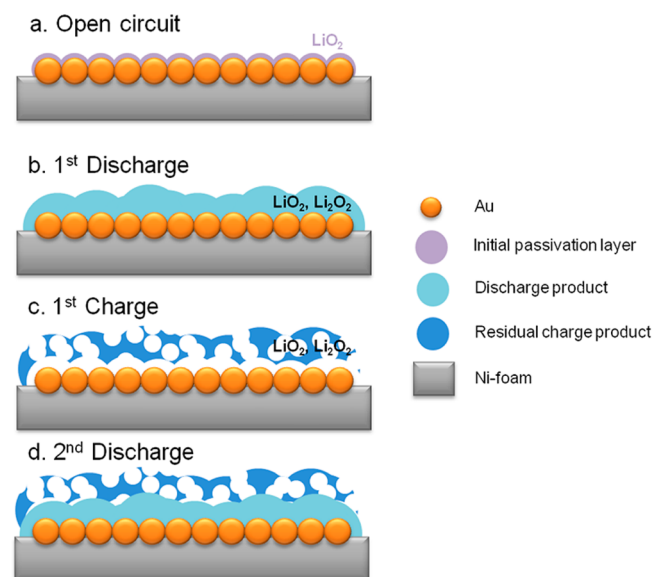

Figure 6. Schematic of an Au−Ni foam electrode surface at different states of charge: (a) open circuit, (b) after discharge, (c) after charge, and (d) after second discharge.

onto the Au surface. A spontaneously formed passivation layer of LiO_2 must be reduced first before further reaction. Discharge reactions are mediated by oxygen adsorption in the form of superoxide followed by spontaneous reaction with free Li^+ ions. Over the course of the discharge, superficial LiO_2 may be further reduced to Li_2O_2 until a sufficiently thick coating of discharge products envelops the Au surface, rendering it inactive. Upon charging, superficial LiO_2 and Li_2O_2 (~1.0 nm) are preferentially oxidized at low overpotentials leaving a large amount of loosely connected residual charge species. In the subsequent discharge cycle, additional LiO_2 and Li_2O_2 are formed at free Au surface sites. As the new layer of discharge products grows (limited by access to the Au surface), residual charge species are pushed further away from the electrode. With each additional cycle, access to the catalyst surface becomes progressively more blocked, resulting in its nearly complete deactivation. In this repeated precipitation and surface-limited oxidation process, we establish a tragically common deactivation mechanism for catalysts in Li−O_2 cells.

■ CONCLUSIONS

This work represents the first truly operando observation of reaction product flux at the catalyst interface of a Li−O_2 electrode by SERS and EIS. Using these methods, we find that LiO_2 forms during discharge and can be further reduced to Li_2O_2 in accordance with the generally accepted mechanism. However, during practical cycling, interfacial LiO_2 is seen to be stable and reversible as it persists through the discharge cycle and is evolved during charging. There are also indications that a passivating layer of LiO_2 forms spontaneously on the Au electrode surface when merely contacted with electrolyte—an

important development when considering the phenomena of the first cycle vs that of subsequent cycles. We observe surface selective oxidation during charging which results in an abundance of residual species in poor contact with the surface. These results provide a rationale for the poor reversibility seen with many metal catalyst systems and may explain the benefit of nanoporous catalyst electrode morphologies which have shown impressive cyclability. Additionally, in situ EIS results confirm the mechanism of formation and oxidation of LiO_2 at reduced overpotentials vs Li_2O_2 by analyzing frequency and potential-dependent real resistance. Using these techniques to focus on phenomena at the electrode interface, our understanding of $Li-O_2$ interfacial reactions and degradation mechanisms can be further improved.

ASSOCIATED CONTENT

Supporting Information

Description of product thickness calculations, Raman peak references and product spectra, supporting ex situ and in situ spectroscopy for cells with DMSO and TEGDME electrolytes (along with supplemental discussion), and additional microscopy showing product morphology. This material is available free of charge via the Internet at http://pubs.acs.org.

AUTHOR INFORMATION

Corresponding Author
*E-mail: andre.taylor@yale.edu.

Notes
The authors declare no competing financial interest.

ACKNOWLEDGMENTS

REFERENCES

(1) Bruce, P. G.; Freunberger, S. A.; Hardwick, L. J.; Tarascon, J.-M. Li-O2 and Li-S Batteries with High Energy Storage. *Nat. Mater.* **2012**, *11*, 19–30.
(2) Girishkumar, G.; McCloskey, B.; Luntz, A. C.; Swanson, S.; Wilcke, W. Lithium-Air Battery: Promise and Challenges. *J. Phys. Chem. Lett.* **2010**, *1*, 2193–2203.
(3) Christensen, J.; Albertus, P.; Sanchez-Carrera, R. S.; Lohmann, T.; Kozinsky, B.; Liedtke, R.; Ahmed, J.; Kojic, A. A Critical Review of Li-Air Batteries. *J. Electrochem. Soc.* **2012**, *159*, R1–R30.
(4) Abraham, K. M.; Jiang, Z. A Polymer Electrolyte-Based Rechargeable Lithium/Oxygen Battery. *J. Electrochem. Soc.* **1996**, *143*, 1–5.
(5) McCloskey, B. D.; Speidel, A.; Scheffler, R.; Miller, D. C.; Viswanathan, V.; Hummelshøj, J. S.; Nørskov, J. K.; Luntz, A. C. Twin Problems of Interfacial Carbonate Formation in Non-Aqueous Li-O2 Batteries. *J. Phys. Chem. Lett.* **2012**, *3*, 997–1001.
(6) McCloskey, B. D.; Bethune, D. S.; Shelby, R. M.; Girishkumar, G.; Luntz, A. C. Solvents' Critical Role in Nonaqueous Lithium-Oxygen Battery Electrochemistry. *J. Phys. Chem. Lett.* **2011**, *2*, 1161–1166.
(7) Thotiyl, M. M. O.; Freunberger, S. A.; Peng, Z.; Bruce, P. G. The Carbon Electrode in Nonaqueous Li-O2 Cells. *J. Am. Chem. Soc.* **2013**, *135*, 494–500.
(8) Freunberger, S. A.; Chen, Y.; Drewett, N. E.; Hardwick, L. J.; Bardé, F.; Bruce, P. G. The Lithium-Oxygen Battery with Ether-Based Electrolytes. *Angew. Chem., Int. Ed.* **2011**, *50*, 8609–8613.
(9) Gittleson, F. S.; Sekol, R. C.; Doubek, G.; Linardi, M.; Taylor, A. D. Catalyst and Electrolyte Synergy in Li-O2 Batteries. *Phys. Chem. Chem. Phys.* **2014**, *16*, 3230–3237.
(10) Laoire, C. O.; Mukerjee, S.; Abraham, K. M.; Plichta, E. J.; Hendrickson, M. A. Influence of Nonaqueous Solvents on the Electrochemistry of Oxygen in the Rechargeable Lithium-Air Battery. *J. Phys. Chem. C* **2010**, *114*, 9178–9186.
(11) Radin, M. D.; Rodriguez, J. F.; Tian, F.; Siegel, D. J. Lithium Peroxide Surfaces Are Metallic, While Lithium Oxide Surfaces Are Not. *J. Am. Chem. Soc.* **2012**, *134*, 1093–1103.
(12) Lu, Y.; Shao-Horn, Y. Probing the Reaction Kinetics of the Charge Reactions of Nonaqueous Li-O2 Batteries. *J. Phys. Chem. Lett.* **2013**, *4*, 93–99.
(13) Viswanathan, V.; Thygesen, K. S.; Hummelshøj, J. S.; Nørskov, J. K.; Girishkumar, G.; McCloskey, B. D.; Luntz, A. C. Electrical Conductivity in Li2O2 and Its Role in Determining Capacity Limitations in Non-Aqueous Li-O2 Batteries. *J. Chem. Phys.* **2011**, *135*, 214704.
(14) Radin, M. D.; Siegel, D. J. Charge Transport in Lithium Peroxide: Relevance for Rechargeable Metal-Air Batteries. *Energy Environ. Sci.* **2013**, *6*, 2370–2379.
(15) Adams, B. D.; Radtke, C.; Black, R.; Trudeau, M. L.; Zaghib, K.; Nazar, L. F. Current Density Dependence of Peroxide Formation in the Li-O2 Battery and Its Effect on Charge. *Energy Environ. Sci.* **2013**, *6*, 1772–1778.
(16) Gallant, B. M.; Kwabi, D. G.; Mitchell, R. R.; Zhou, J.; Thompson, C. V.; Shao-Horn, Y. Influence of Li2O2 Morphology on Oxygen Reduction and Evolution Kinetics in Li-O2 Batteries. *Energy Environ. Sci.* **2013**, *6*, 2518–2528.
(17) Lu, Y.-C.; Kwabi, D. G.; Yao, K. P. C.; Harding, J. R.; Zhou, J.; Zuin, L.; Shao-Horn, Y. The Discharge Rate Capability of Rechargeable Li-O2 Batteries. *Energy Environ. Sci.* **2011**, *4*, 2999–3007.
(18) Xu, J.-J.; Wang, Z.-L.; Xu, D.; Zhang, L.-L.; Zhang, X.-B. Tailoring Deposition and Morphology of Discharge Products towards High-Rate and Long-Life Lithium-Oxygen Batteries. *Nat. Commun.* **2013**, *4*, 1–10.
(19) Gallant, B. M.; Mitchell, R. R.; Kwabi, D. G.; Zhou, J.; Zuin, L.; Thompson, C. V.; Shao-Horn, Y. Chemical and Morphological Changes of Li-O2 Battery Electrodes upon Cycling. *J. Phys. Chem. C* **2012**, *116*, 20800–20805.
(20) Zhong, L.; Mitchell, R. R.; Liu, Y.; Gallant, B. M.; Thompson, C. V.; Huang, J. Y.; Mao, S. X.; Shao-Horn, Y. In Situ Transmission Electron Microscopy Observations of Electrochemical Oxidation of Li2O2. *Nano Lett.* **2013**, *13*, 2209–2214.
(21) Wen, R.; Byon, H. R. In Situ Monitoring of the Li-O2 Electrochemical Reaction on Nanoporous Gold Using Electrochemical AFM. *Chem. Commun.* **2014**, *50*, 2628–2631.
(22) Wen, R.; Hong, M.; Byon, H. R. In Situ AFM Imaging of Li-O2 Electrochemical Reaction on Highly Oriented Pyrolytic Graphite with Ether-Based Electrolyte. *J. Am. Chem. Soc.* **2013**, *135*, 10870–10876.
(23) Lu, Y.-C.; Crumlin, E. J.; Veith, G. M.; Harding, J. R.; Mutoro, E.; Baggetto, L.; Dudney, N. J.; Liu, Z.; Shao-Horn, Y. In Situ Ambient Pressure X-Ray Photoelectron Spectroscopy Studies of Lithium-Oxygen Redox Reactions. *Sci. Rep.* **2012**, *2*, 715.

19024

dx.doi.org/10.1021/am504900k | *ACS Appl. Mater. Interfaces* 2014, 6, 19017–19025

(24) Lu, Y.-C.; Crumlin, E. J.; Carney, T. J.; Baggetto, L.; Veith, G. M.; Dudney, N. J.; Liu, Z.; Shao-Horn, Y. Influence of Hydrocarbon and CO_2 on the Reversibility of Li-O_2 Chemistry Using In Situ Ambient Pressure X-Ray Photoelectron Spectroscopy. *J. Phys. Chem. C* **2013**, *117*, 25948−25954.

(25) Peng, Z.; Freunberger, S. A.; Hardwick, L. J.; Chen, Y.; Giordani, V.; Bardé, F.; Novák, P.; Graham, D.; Tarascon, J.-M.; Bruce, P. G. Oxygen Reactions in a Non-Aqueous Li$^+$ Electrolyte. *Angew. Chem., Int. Ed. Engl.* **2011**, *50*, 6351−6355.

(26) Li, C.; Fontaine, O.; Freunberger, S. A.; Johnson, L.; Grugeon, S.; Bruce, P. G.; Armand, M. Aprotic Li-O_2 Battery: Influence of Complexing Agents on Oxygen Reduction in an Aprotic Solvent. *J. Phys. Chem. C* **2014**, *118*, 3393−3401.

(27) Bañares, M. A. Operando Methodology: Combination of In Situ Spectroscopy and Simultaneous Activity Measurements Under Catalytic Reaction Conditions. *Catal. Today* **2005**, *100*, 71−77.

(28) McCloskey, B.; Bethune, D.; Shelby, R.; Mori, T.; Scheffler, R.; Speidel, A.; Sherwood, M.; Luntz, A. Limitations in Rechargeability of Li-O_2 Batteries and Possible Origins. *J. Phys. Chem. Lett.* **2012**, *3*, 3043−3047.

(29) McCloskey, B. D.; Valery, A.; Luntz, A. C.; Gowda, S. R.; Wallraff, G. M.; Garcia, J. M.; Mori, T.; Krupp, L. E. Combining Accurate O_2 and Li_2O_2 Assays to Separate Discharge and Charge Stability Limitations in Nonaqueous Li-O_2 Batteries. *J. Phys. Chem. Lett.* **2013**, *4*, 2989−2993.

(30) Peng, Z.; Freunberger, S. A.; Chen, Y.; Bruce, P. G. A Reversible and Higher-Rate Li-O_2 Battery. *Science* **2012**, *337*, 563−566.

(31) Lu, Y.-C.; Gasteiger, H. A.; Shao-Horn, Y. Catalytic Activity Trends of Oxygen Reduction Reaction for Nonaqueous Li-Air Batteries. *J. Am. Chem. Soc.* **2011**, *133*, 19048−19051.

(32) Shao, Y.; Park, S.; Xiao, J.; Zhang, J.; Wang, Y.; Liu, J. Electrocatalysts for Nonaqueous Lithium-Air Batteries: Status, Challenges, and Perspective. *ACS Catal.* **2012**, *2*, 844−857.

(33) Ryu, W.; Yoon, T.; Song, S. H.; Jeon, S.; Park, Y.; Kim, I. Bifunctional Composite Catalysts Using Co_3O_4 Nanofibers Immobilized on Nonoxidized Graphene Nanoflakes for High-Capacity and Long-Cycle Li-O_2 Batteries. *Nano Lett.* **2013**, *13*, 4190−4197.

(34) Yilmaz, E.; Yogi, C.; Yamanaka, K.; Ohta, T.; Byon, H. R. Promoting Formation of Noncrystalline Li_2O_2 in the Li-O_2 Battery with RuO_2 Nanoparticles. *Nano Lett.* **2013**, *13*, 4679−4684.

(35) Li, F.; Tang, D.-M.; Chen, Y.; Golberg, D.; Kitaura, H.; Zhang, T.; Yamada, A.; Zhou, H. Ru/ITO: A Carbon-Free Cathode for Nonaqueous Li-O_2 Battery. *Nano Lett.* **2013**, *13*, 4702−4707.

(36) Lu, Y.-C.; Xu, Z.; Gasteiger, H. A.; Chen, S.; Hamad-Schifferli, K.; Shao-Horn, Y. Platinum-Gold Nanoparticles: A Highly Active Bifunctional Electrocatalyst for Rechargeable Lithium-Air Batteries. *J. Am. Chem. Soc.* **2010**, *132*, 12170−12171.

(37) Lim, H.-D.; Song, H.; Gwon, H.; Park, K.-Y.; Kim, J.; Bae, Y.; Kim, H.; Jung, S.-K.; Kim, T.; Kim, Y. H.; Lepró, X.; Ovalle-Robles, R.; Baughmand, R. H.; Kang, K. A New Catalyst-Embedded Hierarchical Air Electrode for High-Performance Li-O_2 Batteries. *Energy Environ. Sci.* **2013**, *6*, 3570−3575.

(38) Tian, Z.; Ren, B.; Wu, D. Surface-Enhanced Raman Scattering: From Noble to Transition Metals and from Rough Surfaces to Ordered Nanostructures. *J. Phys. Chem. B* **2002**, *106*, 9463−9483.

(39) Kneipp, K.; Wang, Y.; Kneipp, H.; Perelman, L.; Itzkan, I.; Dasari, R.; Feld, M. Single Molecule Detection Using Surface-Enhanced Raman Scattering (SERS). *Phys. Rev. Lett.* **1997**, *78*, 1667−1670.

(40) Desilvestro, J.; Weaver, M. Surface Structural Changes During Oxidation of Gold Electrodes in Aqueous Media as Detected Using Surface-Enhanced Raman Spectroscopy. *J. Electroanal. Chem.* **1986**, *209*, 377−386.

(41) Schröter, C.; Roelfs, B.; Solomun, T. The Interaction of Dimethylsulfoxide with a Gold Surface. *Surf. Sci.* **1997**, *380*, L441−L445.

(42) Shen, A.; Pemberton, J. E. Interfacial Structure of Dimethylsulfoxide at Ag Electrodes from Surface Enhanced Raman Scattering and Differential Capacitance. *J. Electroanal. Chem.* **1999**, *479*, 21−31.

(43) Dedryvère, R.; Gireaud, L.; Grugeon, S.; Laruelle, S.; Tarascon, J.-M.; Gonbeau, D. Characterization of Lithium Alkyl Carbonates by X-Ray Photoelectron Spectroscopy: Experimental and Theoretical Study. *J. Phys. Chem. B* **2005**, *109*, 15868−15875.

(44) Lee, H.; Lee, D. J.; Lee, J.-N.; Song, J.; Lee, Y.; Ryou, M.-H.; Park, J.-K.; Lee, Y. M. Chemical Aspect of Oxygen Dissolved in a Dimethyl Sulfoxide-Based Electrolyte on Lithium Metal. *Electrochim. Acta* **2014**, *123*, 419−425.

(45) Zhai, D.; Wang, H.-H.; Yang, J.; Lau, K. C.; Li, K.; Amine, K.; Curtiss, L. A. Disproportionation in Li-O_2 Batteries Based on a Large Surface Area Carbon Cathode. *J. Am. Chem. Soc.* **2013**, *135*, 15364−15372.

(46) Yang, J.; Zhai, D.; Wang, H.-H.; Lau, K. C.; Schlueter, J. A.; Du, P.; Myers, D. J.; Sun, Y.-K.; Curtiss, L. A.; Amine, K. Evidence for Lithium Superoxide-Like Species in the Discharge Product of a Li-O_2 Battery. *Phys. Chem. Chem. Phys.* **2013**, *15*, 3764−3771.

(47) Sharon, D.; Afri, M.; Noked, M.; Garsuch, A.; Frimer, A. A.; Aurbach, D. Oxidation of Dimethyl Sulfoxide Solutions by Electrochemical Reduction of Oxygen. *J. Phys. Chem. Lett.* **2013**, *4*, 3115−3119.

(48) Mozhzhukhina, N.; Méndez De Leo, L. P.; Calvo, E. J. Infrared Spectroscopy Studies on Stability of Dimethyl Sulfoxide for Application in a Li-Air Battery. *J. Phys. Chem. C* **2013**, *117*, 18375−18380.

(49) Younesi, R.; Norby, P.; Vegge, T. A New Look at the Stability of Dimethyl Sulfoxide and Acetonitrile in Li-O_2 Batteries. *ECS Electrochem. Lett.* **2014**, *3*, A15−A18.

(50) Kwabi, D. G.; Batcho, T. P.; Amanchukwu, C. V.; Ortiz-Vitoriano, N.; Hammond, P.; Thompson, C. V.; Shao-Horn, Y. Chemical Instability of Dimethyl Sulfoxide in Lithium-Air Batteries. *J. Phys. Chem. Lett.* **2014**, *5*, 2850−2856.

(51) Zhai, D.; Wang, H.; Lau, K. C.; Gao, J.; Redfern, P. C.; Kang, F.; Li, B.; Indacochea, E.; Das, U.; Sun, H.; Amine, K.; Curtiss, L. A. Raman Evidence for Late Stage Disproportionation in a Li-O_2 Battery. *J. Phys. Chem. Lett.* **2014**, *5*, 2705−2710.

(52) Sathiya, M.; Rousse, G.; Ramesha, K.; Laisa, C. P.; Vezin, H.; Sougrati, M. T.; Doublet, M.-L.; Foix, D.; Gonbeau, D.; Walker, W.; Prakash, A. S.; Ben Hassine, M.; Dupont, L.; Tarascon, J.-M. Reversible Anionic Redox Chemistry in High-Capacity Layered-Oxide Electrodes. *Nat. Mater.* **2013**, *12*, 827−835.

(53) Campbell, C. T. An XPS Study of Molecularly Chemisorbed Oxygen on Ag(111). *Surf. Sci.* **1986**, *173*, L641−L646.

(54) Prabhakaran, K.; Rao, C. A Combined EELS-XPS Study of Molecularly Chemisorbed Oxygen on Silver Surfaces: Evidence for Superoxo and Peroxo Species. *Surf. Sci.* **1987**, *186*, L575−L580.

(55) Yao, K. P. C.; Kwabi, D. G.; Quinlan, R. A.; Mansour, A. N.; Grimaud, A.; Lee, Y.-L.; Lu, Y.-C.; Shao-Horn, Y. Thermal Stability of Li_2O_2 and Li_2O for Li-Air Batteries: In Situ XRD and XPS Studies. *J. Electrochem. Soc.* **2013**, *160*, A824−A831.

(56) Adams, J.; Karulkar, M.; Anandan, V. Evaluation and Electrochemical Analyses of Cathodes for Lithium-Air Batteries. *J. Power Sources* **2013**, *239*, 132−143.

(57) Mogni, L.; Grunbaum, N.; Prado, F.; Caneiro, A. Oxygen Reduction Reaction on Ruddlesden−Popper Phases Studied by Impedance Spectroscopy. *J. Electrochem. Soc.* **2011**, *158*, B202−B207.

(58) Escudero, M. J.; Aguadero, A.; Alonso, J. A.; Daza, L. A Kinetic Study of Oxygen Reduction Reaction on La_2NiO_4 Cathodes by Means of Impedance Spectroscopy. *J. Electroanal. Chem.* **2007**, *611*, 107−116.

(59) Dathar, G. K. P.; Shelton, W. A.; Xu, Y. Trends in the Catalytic Activity of Transition Metals for the Oxygen Reduction Reaction by Lithium. *J. Phys. Chem. Lett.* **2012**, *3*, 891−895.

(60) Xu, Y.; Shelton, W. A. O_2 Reduction by Lithium on Au(111) and Pt(111). *J. Chem. Phys.* **2010**, *133*, 024703.

(61) Yoon, B.; Hakkinen, H.; Landman, U. Interaction of O_2 with Gold Clusters: Molecular and Dissociative Adsorption. *J. Phys. Chem. A* **2003**, *107*, 4066−4071.

(62) Woodham, A. P.; Meijer, G.; Fielicke, A. Charge Separation Promoted Activation of Molecular Oxygen by Neutral Gold Clusters. *J. Am. Chem. Soc.* **2013**, *135*, 1727−1730.

19025

dx.doi.org/10.1021/am504900k | *ACS Appl. Mater. Interfaces* 2014, 6, 19017−19025